Observation of charmed strange meson pair production in $\Upsilon(2S)$ decays and in e^+e^- annihilation at $\sqrt{s} = 10.52$ GeV

B. S. Gao, W. J. Zhu, X. L. Wang, I. Adachi, H. Aihara, D. M. Asner, V. Aulchenko, T. Aushev, R. Ayad, V. Babu[®], Sw. Banerjee[®], M. Bauer[®], P. Behera[®], K. Belous[®], J. Bennett[®], M. Bessner[®], V. Bhardwaj[®], T. Bilka[®], D. Biswas[®], A. Bobrov[®], D. Bodrov[®], A. Bondar[®], A. Bozek[®], M. Bračko[®], P. Branchini[®], T. E. Browder[®], A. Budano, D. Červenkov, M.-C. Chang, P. Chang, V. Chekelian, B. G. Cheon, K. Chilikin, H. E. Cho, K. Cho[®], S.-K. Choi[®], Y. Choi[®], S. Choudhury[®], D. Cinabro[®], G. De Nardo[®], G. De Pietro[®], R. Dhamija[®], F. Di Capua[®], J. Dingfelder[®], Z. Doležal[®], T. V. Dong[®], P. Ecker[®], T. Ferber[®], D. Ferlewicz[®], B. G. Fulsom[®], V. Gauro, A. Girio, E. Grazianio, T. Guo, K. Gudkovao, C. Hadjivasiliouo, K. Hayasakao, H. Hayashiio, S. Hazrao, M. T. Hedges, D. Herrmann, W.-S. Hou, C.-L. Hsu, T. Iijima, K. Inami, N. Ipsita, A. Ishikawa, R. Itoh, M. Iwasaki[®], W. W. Jacobs[®], E.-J. Jang[®], S. Jia[®], Y. Jin[®], K. K. Joo[®], T. Kawasaki[®], C. Kiesling[®], C. H. Kim[®], D. Y. Kim[®], K.-H. Kim[®], Y.-K. Kim[®], K. Kinoshita[®], P. Kodyš[®], T. Konno[®], A. Korobov[®], S. Korpar[®], P. Križan[®], M. Kumar[®], R. Kumar[®], K. Kumara[®], A. Kuzmin[®], Y.-J. Kwon[®], Y.-T. Lai[®], S. C. Lee[®], D. Levit[®], P. Lewis[®], L. K. Li, L. Li Gioi, J. Libby, K. Lieret, D. Liventsev, Y. Ma, M. Masuda, T. Matsuda, S. K. Maurya, F. Meier[®], M. Merola[®], R. Mizuk[®], I. Nakamura[®], M. Nakao[®], D. Narwal[®], A. Natochii[®], L. Nayak[®], M. Niiyama[®], N. K. Nisar[®], S. Nishida[®], S. Ogawa[®], P. Pakhlov[®], G. Pakhlova[®], S. Pardi[®], J. Park[®], S. Patra[®], S. Paul[®], T. K. Pedlar, R. Pestotnik, L. E. Piilonen, T. Podobnik, E. Prencipe, M. T. Prim, G. Russo, S. Sandilya, V. Savinov[®], G. Schnell[®], C. Schwanda[®], Y. Seino[®], K. Senyo[®], M. E. Sevior[®], W. Shan[®], C. Sharma[®], J.-G. Shiu[®], B. Shwartz[®], E. Solovieva[®], M. Starič[®], Z. S. Stottler[®], M. Sumihama[®], K. Tanida[®], F. Tenchini[®], M. Uchida[®], T. Uglovo, Y. Unnoo, S. Unoo, S. E. Vahseno, K. E. Varvello, D. Wango, E. Wango, M.-Z. Wango, S. Watanukio, E. Won, X. Xu, B. D. Yabsley, W. Yan, S. B. Yang, J. H. Yin, Y. Yook, C. Z. Yuan, L. Yuan[®], V. Zhilich[®], and V. Zhukova[®]

(Belle Collaboration)

(Received 17 August 2023; accepted 3 November 2023; published 28 December 2023)

We observe the process $\Upsilon(2S) \to D_s^{(*)+}D_{sJ}^-$ and continuum production $e^+e^- \to D_s^{(*)+}D_{sJ}^-$ at $\sqrt{s}=10.52$ GeV (and their charge conjugates) using the data samples collected by the Belle detector at KEKB, where D_{sJ}^- is $D_{s1}(2536)^-$ or $D_{s2}^*(2573)^-$. Both D_{sJ}^- states are identified through their decay into $\bar{K}\bar{D}^{(*)}$. We measure the products of branching fractions $\mathcal{B}(\Upsilon(2S) \to D_s^{(*)+}D_{sJ}^-)\mathcal{B}(D_{sJ}^- \to \bar{K}\bar{D}^{(*)})$ and the Born cross sections $\sigma^{\text{Born}}(e^+e^- \to D_s^{(*)+}D_{sJ}^-)\mathcal{B}(D_{sJ}^- \to \bar{K}\bar{D}^{(*)})$, and then compare the ratios $R_1 \equiv \mathcal{B}(\Upsilon(2S) \to D_s^{(*)+}D_{sJ}^-)/\mathcal{B}(\Upsilon(2S) \to \mu^+\mu^-)$ for $\Upsilon(2S)$ decays and $R_2 \equiv \sigma^{\text{Born}}(e^+e^- \to D_s^{(*)+}D_{sJ}^-)/\sigma^{\text{Born}}(e^+e^- \to \mu^+\mu^-)$ for continuum production. We obtain $R_1/R_2 = 9.7 \pm 2.3 \pm 1.1$, $6.8 \pm 2.1 \pm 0.8$, $10.2 \pm 3.3 \pm 2.5$, and $3.4 \pm 2.1 \pm 0.8$ for the $D_s^+D_{s1}(2536)^-$, $D_s^*D_{s1}(2536)^-$, $D_s^*D_{s2}^*(2573)^-$, and $D_s^{*+}D_{s2}^*(2573)^-$ final states in the $D_{sJ}^- \to K^-\bar{D}^{(*)0}$ modes, respectively. The measured R_1/R_2 values indicate that the strong decay dominates in $\Upsilon(2S) \to D_s^{(*)+}D_{sJ}^-$ processes. We also measure the ratios of branching fractions $\mathcal{B}(D_{s1}(2536)^- \to K_s^0D^*(2010)^-)/\mathcal{B}(D_{s1}(2536)^- \to K^-D^*(2007)^0) = 0.48 \pm 0.07 \pm 0.02$ and $\mathcal{B}(D_{s2}^*(2573)^- \to K_s^0D^-)/\mathcal{B}(D_{s2}^*(2573)^- \to K^-D^0) = 0.49 \pm 0.10 \pm 0.02$, which are consistent with isospin symmetry. The second ratio is the first measurement of this quantity. Here, the first uncertainties are statistical and the second are systematic.

DOI: 10.1103/PhysRevD.108.112015

Published by the American Physical Society under the terms of the Creative Commons Attribution 4.0 International license. Further distribution of this work must maintain attribution to the author(s) and the published article's title, journal citation, and DOI. Funded by SCOAP³.

I. INTRODUCTION

Much of the plethora of new quarkonium states observed in the last decades has been studied at electron-positron colliders [1]. Experiments at these colliders have collected large data samples at c.m. energies (\sqrt{s}) corresponding to both the vector charmonium and the vector bottomonium

states, which are produced copiously due to resonance enhancements in the cross sections. A vector quarkonium state decays electromagnetically through the annihilation process into a virtual photon or into three gluons mediated by the strong interaction. We can study the dynamics of electromagnetic charmed meson production through complementary measurements at energies above or below the quarkonium state, which are called "off resonance." Here, only quantum electrodynamics (QED) processes contribute and thus allow measurements free from hadronic structure effects and quantum chromodynamics (QCD) related processes present for heavy quarkonia.

At \sqrt{s} significantly above the production threshold and far from quarkonium resonances, the production rates of $e^+e^- \rightarrow q\bar{q}$ are approximately proportional to the quark charge squared, so that $e^+e^- \rightarrow c\bar{c}$ is about 40% of the total hadronic production at $\sqrt{s} = 10.52$ GeV [60 MeV below the $\Upsilon(4S)$]. This provides an opportunity to study the charmed hadrons, including charmed mesons, charmed strange mesons, and charmed baryons. However, this kind of study has not been previously carried out. This is also the case for the Okubo-Zweig-Iizuka suppressed hadronic decays of the narrow $\Upsilon(nS)$ states; hundreds of millions of $\Upsilon(nS)$ events have been accumulated at Belle and BABAR, but such studies are limited. The open charm content of bottomonium hadronic decays can be used as a tool to probe the post- $b\bar{b}$ -annihilation fragmentation processes [2]. Within a QCD approach, the charm quarks are expected to be produced in $\Upsilon(nS)$ decay only by a process in which a virtual timelike gluon of large invariant mass is produced in the initial decay process and subsequently decays into a pair of charmed hadrons [3]. Using a data sample of $(98.6 \pm 0.9) \times 10^6 \Upsilon(2S)$ events, BABAR measures $\mathcal{B}[\Upsilon(1S) \to D^{*+}X] = (2.52 \pm 0.13 \pm 0.15)\%$ [4], which is considerably larger than what is expected from bb annihilation into a single photon. This excess is in agreement with a prediction based on splitting a virtual photon [5], but appears too small to accommodate an octetstate contribution [6]. Here and hereinafter, the first uncertainty quoted is statistical, while the second corresponds to the total systematic uncertainty. However, there are no other measurements of charm hadrons in $\Upsilon(nS)$ decays [7]. It is argued that the suppression of charm production on the $\Upsilon(nS)$ resonance is at least consistent with the analogous case of strangeness production on ψ and $\psi(2S)$, and it would be quite instructive to study the topology of events in which charm is produced [8].

Here, we present searches for $D_s^{(*)+}D_{sJ}^-$ with the subsequent decay $D_{sJ}^- \to \bar{K} + \bar{D}^{(*)}$ in $\Upsilon(2S)$ decays and continuum e^+e^- annihilation, using data recorded with the Belle detector operated at the KEKB asymmetric-energy e^+e^- collider [9]. Charge-conjugated modes are implicitly included throughout the paper. For the $\Upsilon(2S)$ data sample, we have collected data corresponding to an integrated

luminosity of 24.7 fb⁻¹ at a c.m. energy corresponding to the $\Upsilon(2S)$ resonance. We determine the number of produced $\Upsilon(2S)$ events to be $(158\pm4)\times10^6$ using inclusive hadronic decays. The continuum production of the final states is determined using an off-resonance data sample collected using an integrated luminosity of 89.5 fb⁻¹ at $\sqrt{s}=10.52$ GeV. We use these two data samples to separate the dynamics of electromagnetic and strong charmed hadron production at the off-resonance energy and the $\Upsilon(2S)$ peak.

We only include the following D_{sJ}^- states, which are both established and emit a kaon in their decay: $D_{s1}(2536)^-$ and $D_{s2}^*(2573)^-$; the kaon can be charged or neutral (K_s^0) . We use the technique of partial reconstruction for the D_{sJ}^- final state: the final state is tagged through the full reconstruction of the $D_s^{(*)+}$, and the recoiling D_{sJ}^- is tagged by a kaon produced in the decay $D_{sJ}^- \to \bar{K} + \bar{D}^{(*)}$. The remaining $\bar{D}^{(*)}$ is observed indirectly through its recoil against the $D_s^{(*)+} - \bar{K}$ system using the known kinematics of the initial state. This circumvents the problem of low efficiencies for reconstructing D mesons associated with the large variety of possible decay processes.

II. THE BELLE DETECTOR AND MONTE CARLO SIMULATION

The Belle detector is a large-solid-angle magnetic spectrometer [10] using a silicon vertex detector, a 50-layer central drift chamber, an array of aerogel threshold Cherenkov counters, a barrel-like arrangement of time-of-flight scintillation counters, and an electromagnetic calorimeter (ECL) composed of CsI(Tl) crystals located inside a superconducting solenoid coil that provides a 1.5 T magnetic field. An iron flux return outside the coil is instrumented to detect $K_{\rm L}^0$ mesons and identify muons. The origin of the coordinate system is defined as the position of the nominal interaction point. In the cylindrical coordinates, the z axis is aligned with the direction opposite the e^+ beam and points along the magnetic field within the solenoid, and r is the radial distance.

We simulate the full chain $\Upsilon(2S)/e^+e^- \to D_s^{(*)+}D_{sJ}^-$, in which D_{sJ}^- is $D_{s1}(2536)^-$ or $D_{s2}^*(2573)^-$, using the EvtGen generator [11]. We simulate the angular distributions of $D_s^{(*)+}D_{sJ}^-$ according to the J^P quantum numbers of $D_s^{(*)+}$ and D_{sJ}^- . Here, we take $J^P=1^-$ for D_s^{*+} according to the recent BESIII measurement [12]. Four decay modes of D_{sJ}^- are simulated: $K^- + \bar{D}^0$, $K_S^0 + D^-$, $K^- + \bar{D}^*(2007)^0$, and $K_S^0 + D^*(2010)^-$. Again, the D mesons $[\bar{D}^0, D^-, \bar{D}^*(2007)^0$, and $D^*(2010)^-$] are not reconstructed but determined in the recoil of the $D_s^{(*)+}$ and the kaon from the D_{sJ}^- decay, so that the decays of D mesons are inclusive. We simulate the response of the Belle detector using a GEANT3-based Monte Carlo (MC) technique [13].

III. EVENT SELECTION CRITERIA AND RECONSTRUCTION

We search for the tagging D_s^+ using six final states: $\phi \pi^+$, $K_s^0 K^+$, $\bar{K}^* (892)^0 K^+$, $\rho^+ \phi$, $\eta \pi^+$, and $\eta' \pi^+$. The decay of D_s^{*+} only proceeds through $D_s^{*+} \to D_s^{*+} \gamma$.

We reconstruct $D_s^{(*)}+D_{sJ}^-$ final states after initially selecting well-measured charged tracks and photon candidates. A well-measured charged track has an impact parameter dr < 1.5 cm in the $r-\phi$ plane with respect to the interaction point and a displacement |dz| < 5 cm in the r-z plane. We require a transverse momentum larger than 0.1 GeV/c. We identify each charged track by combining the information from different detector subsystems and form the likelihood \mathcal{L}_i [14] for each particle species i, denoting π or K. Tracks with $\mathcal{R}_K = \frac{\mathcal{L}_K}{\mathcal{L}_K + \mathcal{L}_\pi} > 0.6$ are treated as kaons, while those with $\mathcal{R}_K < 0.4$ are assumed to be pions. The identification efficiency is about 95% for both K and π , with a 5% misidentification probability. Photons are identified as ECL clusters that do not align with any charged track.

We reconstruct the K_S^0 , ϕ , $\bar{K}^*(892)^0$, and ρ^+ candidates in their respective decay channels into $\pi^+\pi^-$, K^+K^- , $K^-\pi^+$, and $\pi^+\pi^0$. For candidate K_S^0 mesons, we use pairs of oppositely charged particles originating from a common vertex and assign the pion-mass hypothesis. We use a multivariate technique to improve the purity of the K_S^0 candidate sample by rejecting combinatorial background [15], which we identify with neural networkbased algorithms [16]. For the invariant mass $(M_{\pi^+\pi^-})$ of $\pi^+\pi^-$ pairs we obtain a resolution of $\sigma \approx 5 \text{ MeV}/c^2$, and we define the signal region for K_S^0 by $|M_{\pi^+\pi^-} - m_{K_S^0}| < 3\sigma$. Here, $m_{K_0^0}$ is the nominal mass of the K_S^0 [7]. Correspondingly, we choose the range of all signal mass windows to have $\Delta m = \pm 3\sigma$ around their respective nominal masses [7], unless stated otherwise. The corresponding resolution for the invariant mass of K^+K^- pairs, $M_{K^+K^-}$, is $\sigma \approx 3.3 \text{ MeV}/c^2$. The $\bar{K}^*(892)^0$ meson has a natural width of 47.3 MeV, which is much larger than the experimental resolution for $K^-\pi^+$ pairs. We define the $\bar{K}^*(892)^0$ signal region to be $|M_{K^-\pi^+} - m_{\bar{K}^*(892)^0}| < 105 \text{ MeV}/c^2$, where $M_{K^-\pi^+}$ is the invariant mass of $K^-\pi^+$ and $m_{\bar{K}^*(892)^0}$ is the nominal mass of $\bar{K}^*(892)^0$ [7]. Since the width of the ρ^+ of about 150 MeV is dominated by the natural width, the signal region is selected by $|M_{\pi^+\pi^0} - m_{\rho^+}| < 200 \text{ MeV}/c^2$, in which $M_{\pi^+\pi^0}$ is the invariant mass of $\pi^+\pi^0$ and m_{ρ^+} is the nominal mass of ρ^+ [7].

We combine pairs of photons to form π^0 candidates. For this, we require the energies of photons (E_γ) from π^0 decays to exceed $E_\gamma > 25$ MeV in the barrel $(32.2^\circ < \theta < 128.7^\circ)$ and $E_\gamma > 50$ MeV in the end caps $(12.0^\circ < \theta < 31.4^\circ)$ or $(131.5^\circ < \theta < 157.1^\circ)$ of the ECL, with the polar angles specified in the laboratory frame. The two-photon mass

resolution for $M_{\gamma\gamma}$ is $\sigma \approx 5~{\rm MeV}/c^2$. We reconstruct η mesons from their decays into $\pi^+\pi^-\pi^0$ and $\gamma\gamma$. In the $\gamma\gamma$ mode, we require $E_{\gamma} > 150~{\rm MeV}$. The corresponding mass resolution for $M_{\pi^+\pi^-\pi^0}$ is $\sigma \approx 4~{\rm MeV}/c^2$ and for $M_{\gamma\gamma}$ the resolution is $\sigma \approx 13.5~{\rm MeV}/c^2$. For the selection of η' candidates, we use a combination of η and $\pi^+\pi^-$ pairs. The invariant mass resolution for $\eta\pi^+\pi^-$ is $\sigma_{\eta\pi^+\pi^-} \approx 5~{\rm MeV}/c^2$.

In Figs. 1(a) and 1(c), we show the combined distribution $M_{\rm h_1h_2}$ of $M_{\phi\pi^+}$, $M_{K_c^0K^+}$, $M_{\bar{K}^*(892)^0K^+}$, $M_{\rho^+\phi}$, $M_{\eta\pi^+}$, and $M_{\eta'\pi^+}$ from the $\Upsilon(2S)$ data sample (upper row) and the continuum data sample (lower row). We do not apply a mass constraint for π^0 , η , or η' . Instead, we take the advantage of the mass difference. Taking the $D_s^+ \to \eta \pi^+$ with $\eta \to \gamma \gamma$ as an example, we use $M_{\eta\pi^+}=M_{\gamma\gamma\pi^+}-M_{\gamma\gamma}+m_{\eta}$, where the invariant mass $M_{\gamma\gamma\pi^+}$ $(M_{\gamma\gamma})$ is calculated from the sum of the 4momenta of $\gamma\gamma\pi^+$ ($\gamma\gamma$). In this way, the mass resolution of the D_s^+ signal in $M_{n\pi^+}$ is improved from 19.7 to 13.0 MeV/ c^2 according to signal MC simulation. We fit the D_s^+ signal in $M_{h_1h_2}$ with a Gaussian function and describe the background through a second-order polynomial function. We obtain a mass resolution of $\sigma_{D_c^+} = 6.7 \pm 0.1 \text{ MeV}/c^2$ in data, which is used to define the signal region for D_s^+ , while the corresponding resolution is $6.5 \text{ MeV}/c^2$ in signal MC simulations. Besides the D_s^+ signal, we also define sideband regions through $|M_{h_1h_2} - m_{D_s^+} \pm 9\sigma_{D_s^+}| < 3\sigma_{D_s^+}$. Since the fraction of multicombination in D_s^+ reconstruction is only about 3%, we allow multiple candidates of D_s^+ in

We reconstruct D_s^{*+} candidates from the above D_s^{+} sample using the γD_s^+ final state. For this, we require the photon energy to exceed $E_{\gamma} > 50$ MeV in the barrel and $E_{\gamma} > 100$ MeV in the end caps of the ECL. The corresponding invariant mass distributions $M_{\gamma D_s^+}$ for γD_s^+ from the $\Upsilon(2S)$ and continuum data samples are shown in Figs. 1(b) and 1(d). Here, we use $M_{\gamma D_s^+} = M_{\gamma h_1 h_2}$ – $M_{h_1h_2} + m_{D_s^+}$, where the invariant mass $M_{\gamma h_1h_2}$ is calculated from the sum of the 4-momenta of $\gamma h_1 h_2$. We fit to the $M_{\gamma D_{\tau}^{+}}$ distribution between 2.07 and 2.15 GeV/ c^{2} using two Gaussian functions for the D_s^{*+} signal and a second-order polynomial function for the background. We use $\sigma \equiv \sqrt{f_1 \times (\sigma_1^2 + m_1^2) + f_2 \times (\sigma_2^2 + m_2^2) - m^2}$ with $m = f_1 \times m_1 + f_2 \times m_2$ to define the mass resolution of the D_s^{*+} signals, where m_1 (m_2), σ_1 (σ_2), and f_1 (f_2) are the mean, the standard deviation, and the fraction of the first (second) Gaussian function. We obtain the mass resolution of $\sigma_{D_{*}^{*+}} = 6.7 \pm 0.4 \text{ MeV}/c^2$ in data and 7.0 MeV/ c^2 in signal MC simulations, which agree well with each other. Again, in addition to the signal region for D_s^{*+} , we define sideband regions through $|M_{\gamma D_s^+} - m_{D_s^{*+}} \pm 9\sigma_{D_s^{*+}}| < 3\sigma_{D_s^{*+}}$. As we aim to study the $D_s^{*+}\bar{K}$ recoil spectrum, we apply mass-constrained

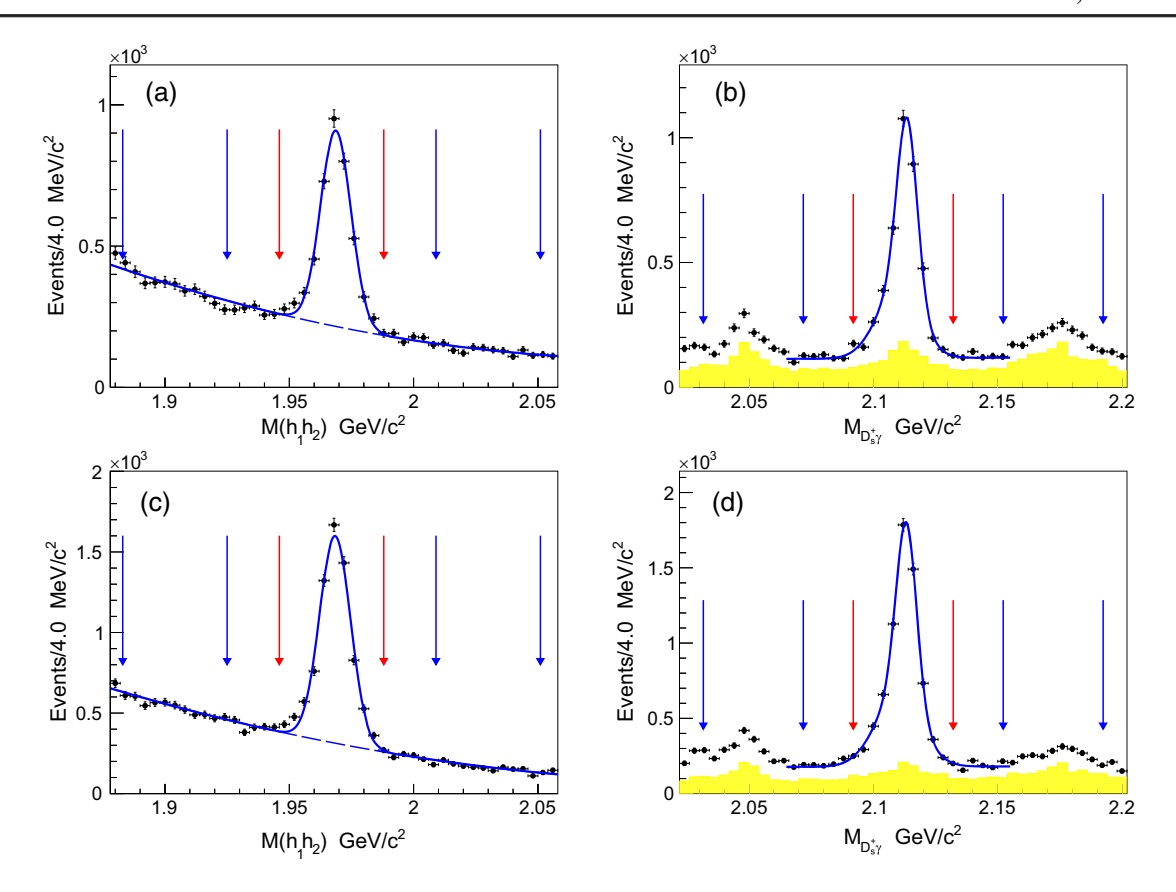


FIG. 1. Invariant mass distributions of (a),(c) the combinations of $\phi\pi^+$, $K_S^0K^+$, $\bar{K}^*(892)^0K^+$, $\rho^+\phi$, $\eta\pi^+$, and $\eta'\pi^+$ for D_s^+ candidates and (b),(d) the combinations of γD_s^+ for $D_s^{(*)+}$ candidates in $\Upsilon(2S)$ data sample (upper row) and continuum data sample (lower row). The red arrows show the signal region of D_s^+ or $D_s^{(*)+}$, and the blue arrows show the sideband regions. The shaded histogram in (b) and (d) shows backgrounds estimated from D_s^+ mass sidebands. The curves show the best fit results using Gaussian functions for the D_s^+ and $D_s^{(*)+}$ signals, respectively.

fits to the D_s^{*+} candidates in the signal region to improve their momentum resolution. We find that 10% of the events have multiple D_s^{*+} candidates. In these cases, we select the candidate with the minimum χ^2 from the massconstraint fit. For the candidates in each D_s^{*+} mass sideband, we apply the mass constraint to the center of the sideband and select the combination with minimum χ^2 as well. To estimate the size of the peaking component in the selected D_s^{*+} sample due to the minimum χ^2 requirement, we apply the same mass constraints to events in the D_s^+ sidebands. As shown in Figs. 1(b) and 1(d), the D_s^+ mass sideband events can describe the peaks in the D_s^{*+} mass sidebands and therefore can be used to estimate reliably the peaking component in the D_s^{*+} mass signal region. Events with $|M_{\gamma D_s^+} - m_{D_s^{*+}}| < 50 \text{ MeV}/c^2$ are removed for the $D_s^+ D_{sJ}^-$

The search for $\bar{D}^{(*)}$ requires a \bar{K} meson reconstructed in addition to $D_s^{(*)+}$. We determine the $\bar{D}^{(*)}$ signal through the recoil of $D_s^{(*)+}\bar{K}$ using the calculated mass,

$$\begin{split} M_{\bar{D}^{(*)}} &= M_{D_s^{(*)+}\bar{K}}^{\text{recoil}} \\ &\equiv \sqrt{(E_{\text{c.m.}} - E_{D_s^{(*)+}} - E_{\bar{K}})^2 - (\vec{p}_{\text{c.m.}} - \vec{p}_{D_s^{(*)+}} - \vec{p}_{\bar{K}})^2}, \end{split}$$

and isolate the possible production of D_{sJ}^- states in the $\bar{K}\bar{D}^{(*)}$ final states through their recoil using the following equation:

$$\begin{split} M_{\bar{K}\bar{D}^{(*)}} &= M_{D_s^{(*)+}}^{\text{recoil}} \\ &\equiv \sqrt{(E_{\text{c.m.}} - E_{D_s^{(*)+}})^2 - (\vec{p}_{\text{c.m.}} - \vec{p}_{D_s^{(*)+}})^2}. \quad (2) \end{split}$$

Here, $E_{\rm c.m.}$ and $\vec{p}_{\rm c.m.}$ are the energy and 3-momentum of e^+e^- in the collision system, $E_{D_s^{(*)+}}$ ($E_{\bar{K}}$) and $\vec{p}_{D_s^{(*)+}}$ ($\vec{p}_{\bar{K}}$) are those of $D_s^{(*)+}$ (\bar{K}), respectively. We show the $M_{D_s^{(*)+}\bar{K}}^{\rm recoil}$ distributions versus $M_{D_s^{(*)+}}^{\rm recoil}$ from the two data samples in Figs. 2(a) and 2(b), and the signal MC simulations of $\Upsilon(2S)$

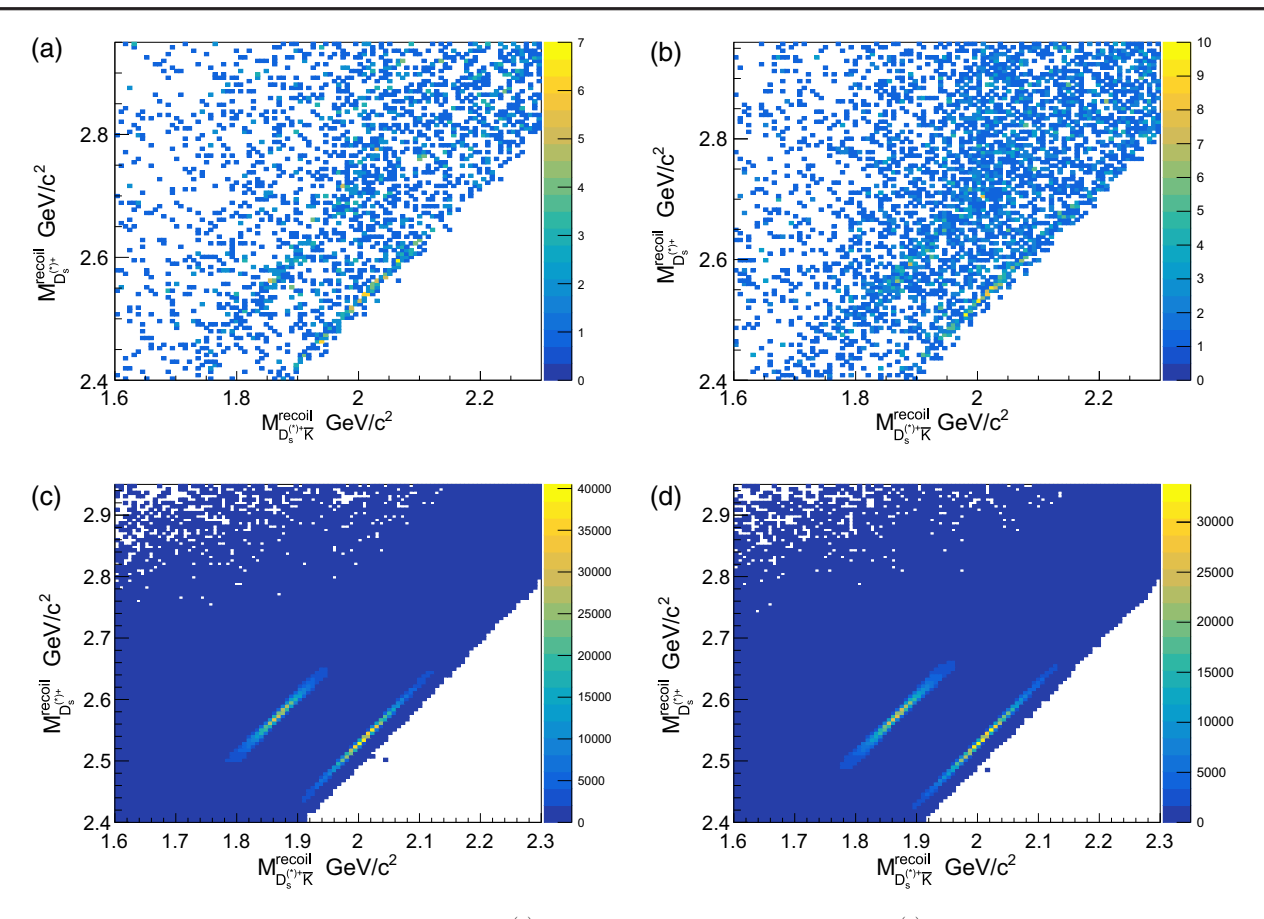


FIG. 2. The distributions of the recoil mass against $D_s^{(*)+}\bar{K}$ versus the recoil mass against $D_s^{(*)+}$ in (a) the $\Upsilon(2S)$ data sample, (b) the continuum data sample at $\sqrt{s}=10.52$ GeV, (c) the signal MC simulation of $\Upsilon(2S)$ decays, and (d) the signal MC simulation of continuum production at $\sqrt{s}=10.52$ GeV.

decays and continuum production in Figs. 2(c) and 2(d). There are clear bands in the distributions of data corresponding to the production of the $D_{s1}(2536)^-$ signal in the $\bar{\bar{D}}^*\bar{K}$ $[\bar{\bar{D}}^*(2007)^0K^-$ or $D^*(2010)^-K_S^0]$ final state and $D_{s2}^*(2573)^-$ signal in the $\bar{D}\bar{K}$ (\bar{D}^0K^- or $D^-K_s^0$) final state, and they agree well with the signal MC simulations. The mass resolutions of $M_{D_s^{(*)+}\bar{K}}^{\text{recoil}}$ and $M_{D_s^{(*)+}}^{\text{recoil}}$ are large due to the common variables $E_{D^{(*)+}}$ and $\vec{p}_{D^{(*)+}}$ in Eqs. (1) and (2). The mass resolution of \bar{D} from the decay of D_{sJ}^- in $M_{D_s^{(*)+}\bar{K}}^{\text{recoil}}$ is about 50 MeV/c^2 , and the signal region is defined to be $|M_{D_s^{(*)+}\bar{K}}^{\rm recoil} - m_{\bar{D}}| < 150 \text{ MeV}/c^2$. We fit the \bar{D}^* mass distribution with two Gaussian functions and obtain the narrower one with a mass resolution of $31.8 \pm$ $0.3 \text{ MeV}/c^2$ and a signal fraction of about 34% and the wider one with a mass resolution of $74.2 \pm 1.0 \text{ MeV}/c^2$ and a signal fraction of about 66%. We define the signal region to be $|M_{D_s^{(*)+}\bar{K}}^{\text{recoil}} - m_{\bar{D}^*}| < 200 \text{ MeV}/c^2$, which has a selection efficiency of about 95%. Here, $m_{\bar{D}}$ is the nominal mass of \bar{D}^0 or D^- , and $m_{\bar{D}^*}$ is the nominal mass of the $\bar{D}^*(2007)^0$ or $D^*(2010)^-$ [7]. With the events in the D_s^+ or

 D_s^{*+} mass sidebands, no peaking background is found for the $\bar{D}^{(*)}$ signal in the $M_{D_s^{(*)+}\bar{K}}^{\mathrm{recoil}}$ distributions.

To improve the mass resolution of $M_{\bar{K}\bar{D}^{(*)}}$, we use the following formula to replace Eq. (2):

$$M_{\tilde{K}\tilde{D}^{(*)}} = M_{D_s^{(*)+}}^{\text{recoil}} - M_{D_s^{(*)+}\tilde{K}}^{\text{recoil}} + m_{\tilde{D}^{(*)}}.$$
 (3)

In this way, the uncertainties due to the 4-momentum of final states from $D_s^{(*)+}$ decays are significantly reduced. From simulation, we obtain the resolutions for $\Delta M^{\text{recoil}} \equiv$

 $M_{D_s^{(*)+}}^{
m recoil} - M_{D_s^{(*)+}ar{K}}^{
m recoil}$ of $\sigma_{\Delta M^{
m recoil}} < 5~{
m MeV}/c^2$ for all $D_s^{(*)+}D_{sJ}^{-}$ final states. In Figs. 3 and 4 we show the distributions for $\Delta M^{
m recoil} + m_{ar{D}^*}$ for $M_{ar{K}ar{D}^*}$ and $\Delta M^{
m recoil} + m_{ar{D}}$ for $M_{ar{K}ar{D}}$ for the two data samples. We observe clear signals for both $D_{s1}(2536)^-$ and $D_{s2}^*(2573)^-$.

We determine the D_{sJ}^- signal yields, $N_{\Upsilon(2S)}^{\rm sig}$ of the $\Upsilon(2S)$ decays and $N_{\rm cont}^{\rm sig}$ of the continuum production at $\sqrt{s}=10.52$ GeV, by simultaneously fitting the $M_{\bar{K}\bar{D}^{(*)}}$ distributions for the $\Upsilon(2S)$ data sample and the continuum data sample and with common isospin ratios

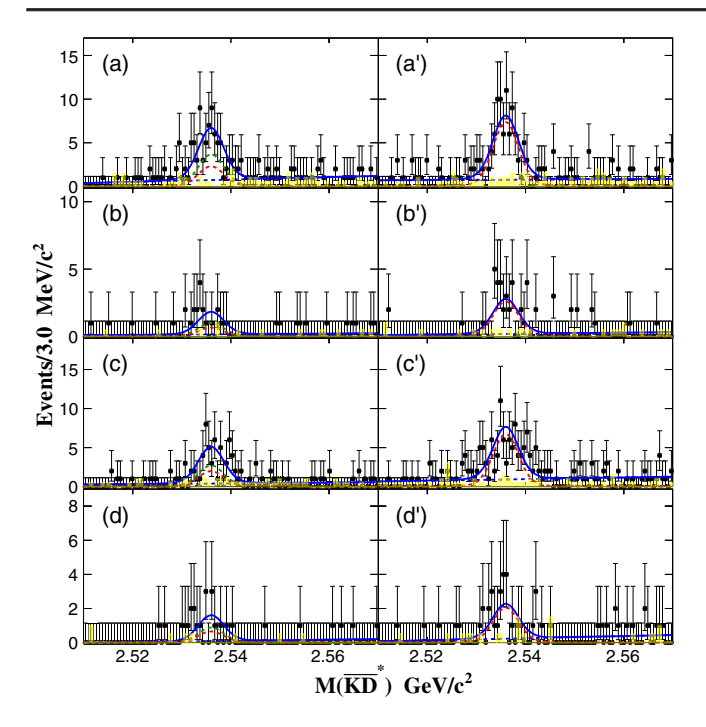


FIG. 3. The invariant mass distributions of $\bar{K}\bar{D}^*$ calculated in the recoil mass for $D_s^{(*)+}$ in the (a) $D_s^+K^-\bar{D}^*(2007)^0$, (b) $D_s^+K_s^0D^*(2010)^-$, (c) $D_s^{*+}K^-\bar{D}^*(2007)^0$, and (d) $D_s^*K_s^0D^*(2010)^-$ final states from the $\Upsilon(2S)$ data sample (a)–(d) and the continuum data sample at 10.52 GeV (a')–(d'). The shaded histograms show the backgrounds estimated from the normalized $D_s^{(*)+}$ mass sidebands. The solid curves show the best fit result; the dashed green ones are $D_{s1}(2536)^-$ signals in $\Upsilon(2S)$ decays, and the dashed red curves are the $D_{s1}(2536)^-$ signals in continuum production at 10.02 GeV (a)–(d) and 10.52 GeV (a')–(d').

 $R_{\mathrm{iso},J}\equiv\mathcal{B}(D_{sJ}^- o K_S^0D^{(*)-})/\mathcal{B}(D_{sJ}^- o K^-ar{D}^{(*)0})$ between the $K_S^0D^{(*)-}$ and $K^-ar{D}^{(*)0}$ final states. In the fits, we use $N_{\Upsilon(2S)}^{\rm sig}$ and $N_{\rm cont}^{\rm sig}$ for the $K^-\bar{D}^{(*)0}$ modes, and those of the $K_{\rm s}^0 D^{(*)-}$ modes are calculated via the isospin ratios $R_{{\rm iso},J}$ and the ratios of efficiencies and branching fractions between the $K_s^0 D^{(*)-}$ modes and the $K^- \bar{D}^{(*)0}$ modes. The fit function is the sum of a Breit-Wigner function (BW) convolved with a Gaussian function with a width corresponding to the mass resolution and a linear function to describe the backgrounds. The mass and width of the BW functions are fixed to the world average values for $D_{s1}(2536)^-$ and $D_{s2}^*(2573)^-$ [7]. The mass resolutions used in the Gaussian are obtained from MC simulations and are about 2.4 MeV/ c^2 (6.5 MeV/ c^2) for $D_{s1}(2536)^ [D_{s2}^*(2573)^-]$. We include the branching fractions and reconstruction efficiencies corresponding to the $D_s^{(*)+}D_{s,l}^$ final states in the fits. The results are listed in Table I for each channel and each dataset.

We estimate the contribution of continuum production to the $D_s^{(*)+}D_{sJ}^-$ signal in the $\Upsilon(2S)$ data sample. For this,

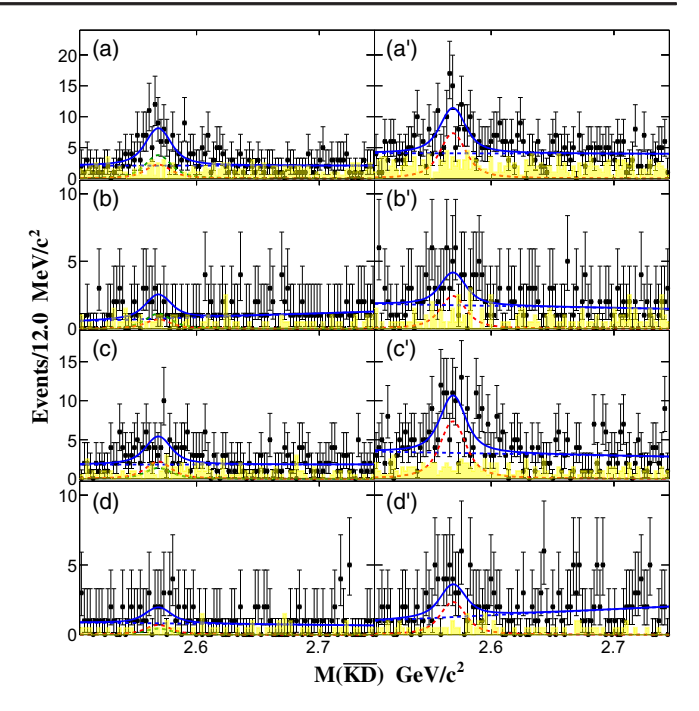


FIG. 4. The invariant mass distributions of $\bar{K}\bar{D}$ calculated in recoil mass for $D_s^{(*)+}$ in the (a) $D_s^+K^-\bar{D}^0$, (b) $D_s^+K_S^0D^-$, (c) $D_s^{*+}K^-\bar{D}^0$, and (d) $D_s^{*+}K_S^0D^-$ final states from the $\Upsilon(2S)$ data sample (a)–(d) and the continuum data sample at 10.52 GeV (a')–(d'). The shaded histograms show the backgrounds estimated from the normalized $D_s^{(*)+}$ mass sidebands. The solid curves show the best fit result; the dashed green ones are $D_{s2}^*(2573)^-$ signals in $\Upsilon(2S)$ decays, and the dashed red curves are the $D_{s2}^*(2573)^-$ signals in continuum production at 10.02 GeV (a)–(d) and 10.52 GeV (a')–(d').

we scale the luminosities and correct for the c.m. energy dependence of the QED cross section $\sigma_{e^+e^-} \propto 1/s$, resulting in a scale factor $f_{\rm scale} = (\mathcal{L}_{\Upsilon(2S)} \times s_{\rm cont})/(\mathcal{L}_{\rm cont} \times s_{\Upsilon(2S)}) = 0.304$. Here, $\mathcal{L}_{\Upsilon(2S)}$ and $\mathcal{L}_{\rm cont}$ are the integrated luminosities of the $\Upsilon(2S)$ data sample at $\sqrt{s_{\Upsilon(2S)}} = 10.02$ GeV and the continuum data sample at $\sqrt{s_{\rm cont}} = 10.52$ GeV. Therefore, the yield of signal events produced via continuum e^+e^- annihilation in the $\Upsilon(2S)$ data sample is $f_{\rm scale} \times N_{\rm cont}^{\rm sig}$.

In principle, there is interference between the resonance and continuum amplitudes in the $\Upsilon(2S)$ data sample [17]. We do not consider this effect in the simultaneous fit but consider it in the systematic uncertainty in Sec. IV.

We determine the statistical significance of D_{sJ}^- by comparing the value of $\Delta(-2\ln L) = -2\ln(L_{\rm max}/L_0)$ and the change in the number of free parameters in the fits, where $L_{\rm max}$ is the likelihood with D_{sJ}^- and L_0 without D_{sJ}^- . The statistical significance in the $\Upsilon(2S)$ data sample for $D_{s1}(2536)^-$ and $D_{s2}^*(2573)^-$ is 6.8σ and 4.0σ , respectively, and 18.3σ and 10.1σ in the continuum data sample. From these yields, we calculate the branching

TABLE I. The branching fractions of $\Upsilon(2S) \to D_s^{(*)+}D_{sJ}^-$ decays, the Born cross sections of continuum production $e^+e^- \to D_s^{(*)+}D_{sJ}^-$, and the isospin ratio $\mathcal{B}(D_{sJ}^- \to K_S^0D^{(*)-})/\mathcal{B}(D_{sJ}^- \to K^-\bar{D}^{(*)0})$ based on the results from the simultaneous fits. Here, $N_{\Upsilon(2S)}^{\text{sig}}$, $N_{\text{cont}}^{\text{sig}}$, $\mathcal{B}(\Upsilon(2S) \to D_s^{(*)+}D_{sJ}^-)\mathcal{B}(D_{sJ}^- \to \bar{K}\bar{D}^{(*)})$, and $\sigma^B(e^+e^- \to D_s^{(*)+}D_{sJ}^-)\mathcal{B}(D_{sJ}^- \to \bar{K}\bar{D}^{(*)})$ are described in Eqs. (4) and (5). $\sum \varepsilon_i \mathcal{B}_i$ is the sum of the products of the reconstruction efficiencies and branching fractions in D_s^+ 's six decay channels. The significance is the statistical significance of the $D_s^{(*)+}D_{sJ}^-$ signals with $D_{sJ}^- \to K^-D^{(*)0}$ and $K_S^0D^{(*)-}$ in $\Upsilon(2S)$ decays and continuum productions. The $K^-D^{(*)0}$ and $K_S^0D^{(*)-}$ modes of the D_{sJ}^- decays are connected by the isospin ratio $\mathcal{B}(D_{sJ}^- \to K_S^0D^{(*)-})/\mathcal{B}(D_{sJ}^- \to K^-\bar{D}^{(*)0})$ in the simultaneous fits. The systematic uncertainties of N^{sig} are of the simultaneous fits only.

$N_{\Upsilon(2S)}^{\mathrm{sig}}$)	Significance .		$\mathcal{B}(\Upsilon(2S) \to D_s^{(*)+} D_{sJ}^-) \mathcal{B}(D_{sJ}^- \to \bar{K}\bar{D}^{(*)}) (\times 10^{-5})$		
Final state (f)	K^- mode	K_S^0 mode	(σ)		K^- mode	K_S^0 mode	
$D_s^+ D_{s1}(2536)^-$	$43 \pm 9 \pm 2$	$14 \pm 3 \pm 2$	5.3	1.	$6 \pm 0.3 \pm 0.2$	$0.84 \pm 0.18 \pm 0.15$	
$D_s^{*+}D_{s1}(2536)^-$	$31 \pm 8 \pm 2$	$10 \pm 3 \pm 2$	4.3	1.	$4 \pm 0.4 \pm 0.2$	$0.82 \pm 0.25 \pm 0.19$	
$D_s^+ D_{s2}^* (2573)^-$	$51\pm15\pm5$	$17\pm5\pm5$	3.8	1.	$4 \pm 0.4 \pm 0.2$	$0.69 \pm 0.20 \pm 0.22$	
$D_s^{*+}D_{s2}^{*}(2573)^-$	$20\pm12\pm2$	$20 \pm 12 \pm 2$ $7 \pm 4 \pm 4$		0.	$9 \pm 0.5 \pm 0.2$	$0.54 \pm 0.31 \pm 0.47$	
	$N_{ m cont}^{ m sig}$				$\sigma^{ m B}(e^+e^- o D_s^{(*)+}D_{sJ}^-){\cal B}(D_{sJ}^- o ar Kar D^{(*)})({ m fl}$		
	K⁻ mode	K_S^0 mode			K⁻ mode	K_S^0 mode	
$D_s^+ D_{s1}(2536)^-$	$86 \pm 10 \pm 2$	$28 \pm 4 \pm 2$	13.9		$67 \pm 8 \pm 6$	$34 \pm 5 \pm 4$	
$D_s^{*+}D_{s1}(2536)^-$	$79 \pm 10 \pm 2$	$25 \pm 4 \pm 2$	11.8		$84\pm11\pm11$	$41 \pm 6 \pm 6$	
$D_s^+ D_{s2}^* (2573)^-$	$102\pm17\pm21$	$33 \pm 8 \pm 5$	7.1		$56 \pm 9 \pm 13$	$27\pm 6\pm 5$	
$D_s^{*+}D_{s2}^{*}(2573)^-$	$102 \pm 16 \pm 6$	$33 \pm 7 \pm 4$	7.6		$106\pm17\pm12$	$51 \pm 11 \pm 9$	
			$\sum \varepsilon_i \mathcal{B}_i$ (%)				
Final state (f)	$D_s^+ D_{s1}(2536)^-$	$D_s^{*+}D_{s1}$	$D_s^{*+}D_{s1}(2536)^-$		$D_s^+ D_{s2}^* (2573)^-$	$D_s^{*+}D_{s2}^*(2573)^-$	
K⁻ mode	1.63 ± 0.07	1.06 =	1.06 ± 0.05		1.19 ± 0.05	0.77 ± 0.03	
K_S^0 mode	2.32 ± 0.10	1.56 =	1.56 ± 0.07		1.22 ± 0.05	0.82 ± 0.03	
Isospin ratio $\mathcal{B}(D_{s,s}^-)$	$K_{S} \rightarrow K_{S}^{0} D^{(*)-})/\mathcal{B}(D_{S}^{-})$	$\rightarrow K^-\bar{D}^{(*)0})$					

 $0.48 \pm 0.07 \pm 0.02$

 $0.49 \pm 0.10 \pm 0.02$

fraction of $\Upsilon(2S) \to D_s^{(*)+} D_{sJ}^-$ and the Born cross section for $e^+e^- \to D_s^{(*)+} D_{sJ}^+$ by

$$\mathcal{B}(\Upsilon(2S) \to D_s^{(*)+} D_{sJ}^-) \mathcal{B}(D_{sJ}^- \to \bar{K} \bar{D}^{(*)})$$

$$= \frac{N_{\Upsilon(2S)}^{\text{sig}}}{N_{\Upsilon(2S)} \times \sum \varepsilon_i \mathcal{B}_i}, \tag{4}$$

and

 $D_{s1}(2536)^-$ decays $D_{s2}^*(2573)^-$ decays

$$\sigma^{\mathrm{B}}(e^{+}e^{-} \to D_{s}^{(*)+}D_{sJ}^{-})\mathcal{B}(D_{sJ}^{-} \to \bar{K}\bar{D}^{(*)})$$

$$= \frac{N_{\mathrm{cont}}^{\mathrm{sig}} \times |1 - \Pi|^{2}}{\mathcal{L}_{\mathrm{cont}} \times \sum \varepsilon_{i}\mathcal{B}_{i} \times (1 + \delta_{\mathrm{ISP}})}.$$
(5)

Here, *i* identifies the mode of $D_s^+ \to h_1 h_2$ decay, while ε_i and \mathcal{B}_i are their reconstruction efficiencies and branching fractions. We calculate $\sum \varepsilon_i \mathcal{B}_i$ according to signal MC simulations for ε_i and the world average values of \mathcal{B}_i [7]

and list the values in Table I. Their errors are mainly due to the uncertainties of \mathcal{B}_i from world averages [7], since all of the relative statistical uncertainties due to the statistics of MC simulations are less than 0.5%. Here, we take into account the branching fraction of $K_s^0 \to \pi^+\pi^-$ decay [7]. From the Born cross sections we can calculate the full "dressed" cross section through $\sigma^{\text{dressed}} = \sigma^{\text{Born}}/|1-\Pi|^2$. The factor $|1-\Pi|^2=0.931$ is the vacuum polarization factor [18,19]. In addition, we have to correct for radiative effects. The radiative correction factor $1+\delta_{\text{ISR}}$ is determined by $\int \sigma^{\text{dressed}}(s(1-x))F(x,s)dx/\sigma^{\text{dressed}}(s)$ and has the value 0.82, where F(x,s) is the radiative function obtained from a QED calculation with an accuracy of 0.2% [20–22].

We summarize the branching fractions of $\Upsilon(2S)$ decays and the Born cross sections of continuum production in Table I. The number of corrected signal events in the $\Upsilon(2S)$ data sample is $20 \pm 12 \pm 2$ for the $D_s^{*+}D_{s2}^*(2573)^-$ decay, from which we derive a statistical significance of only 1.6σ .

We integrate the likelihood versus the number of $D_s^{*+}D_{s2}^*(2573)^-$ signal events and determine its upper limit at 90% confidence level (C.L.) to be $N^{\rm UL}(\Upsilon(2S) \to D_s^{*+}D_{s2}^*(2573)^-) < 44$ in the $D_{s2}^*(2573)^- \to K^-\bar{D}^0$ mode, which has been degraded by a factor of $1/(1-\delta_{\rm sys})$ to account for the systematic uncertainties detailed below. We obtain an upper limit for the production in $\Upsilon(2S)$ decay of $\mathcal{B}^{\rm UL}(\Upsilon(2S) \to D_s^{*+}D_{s2}^*(2573)^-)\mathcal{B}(D_{s2}^*(2573)^- \to K^-\bar{D}^0) < 2.9 \times 10^{-5}$.

In addition, we determine the isospin ratios $R_{iso,J}$ from the simultaneous fits to be $R_{\rm iso,1} = 0.48 \pm 0.07 \pm 0.02$ and $R_{\rm iso,2} = 0.49 \pm 0.10 \pm 0.02$ for the $D_{s1}(2536)^-$ and $D_{s2}^{*}(2573)^{-}$, respectively. These ratios are in good agreement with the expectation from isospin symmetry, which are 0.498 and 0.497 from a calculation taking into account the phase space. Replacing the $N_{\Upsilon(2S)}^{\rm sig}$ and $N_{\rm cont}^{\rm sig}$ of $K^-\bar{D}^{(*)0}$ modes with those of the $K_S^0 D^{(*)-}$ modes in the simultaneous fits, and calculating those of the $K^{-}\bar{D}^{(*)0}$ modes with $R_{iso,J}$ and the ratios of efficiencies and branching fractions between the $K^-\bar{D}^{(*)0}$ modes and the $K_s^0D^{(*)-}$ modes, we obtain the new fit results and calculate the $\mathcal{B}(\Upsilon(2S) \to D_s^{(*)+}D_{sJ}^-)\mathcal{B}(D_{sJ}^- \to \bar{K}\bar{D}^{(*)})$ and $\sigma^{\mathrm{B}}(e^+e^- \to 0)$ $D_s^{(*)+}D_{sJ}^-)\mathcal{B}(D_{sJ}^-\to \bar{K}\bar{D}^{(*)})$ of the $D_{sJ}^-\to K_S^0D^{(*)-}$ decay modes, as listed in Table I. We get the same fit results of the isospin ratios $R_{iso,J}$ of the $D_{s1}(2536)^-$ and $D_{s2}^*(2573)^-$ decays. We also determine the $N^{\rm UL}(\Upsilon(2S) \to D_s^{*+}D_{s2}^*(2573)^-) < 15$ in the $K_S^0D^-$ mode and $\mathcal{B}^{\rm UL}(\Upsilon(2S) \to D_s^{*+}D_{s2}^*(2573)^-)\mathcal{B}(D_{s2}^*(2573)^- \to K_S^0D^-) < 3.0 \times 10^{-5}$ at 90% C.L.

IV. SYSTEMATIC UNCERTAINTIES

The determination of the branching fractions in $\Upsilon(2S)$ decays and the Born cross sections of continuum productions have various systematic uncertainties, which are listed in Table II. The particle identification uncertainty for K^{\pm} is 1.1% and 0.9% per π^{\pm} [14]; the uncertainty of the tracking efficiency per track is 0.35% and is added linearly; the photon reconstruction uncertainty is 2% for each photon. The uncertainties of the efficiency of mass window requirements due to data and MC differences in mass resolutions for π^0 , K_S^0 , $\bar{K}^*(892)^0$, ρ^+ , ϕ , η , and η' are measured to be 0.2%, 0.2%, 1.0%, 1.4%, 0.1%, 1.7%, and 0.3%, respectively. We take the decay branching fractions and their uncertainties of the intermediate states $\bar{K}^*(892)^0$, η , ρ^+ , η' , and $D_s^{(*)+}$ from Ref. [7]. We determine the efficiency of the D_s^+ (D_s^{*+}) mass window to be (99.9 \pm 0.1)% $[(99.8 \pm 0.1)\%]$ in data and 97.4% (99.5%) in the simulation, and we attribute a systematic uncertainty of 2.5% (0.3%); the differences in these numbers for data and simulation reflect the different mass resolutions obtained

TABLE II. The summary of systematic uncertainties (%) of $D_s^{(*)+}K$ reconstruction. Additional uncertainties due to the angular distributions are 6.9%, 8.5%, 8.5%, and 9.2% for the $D_s^+D_{s1}(2536)^-$, $D_s^+D_{s2}^*(2573)^-$, $D_s^{*+}D_{s1}(2536)^-$, and $D_s^{*+}D_{s2}^*(2573)^-$, respectively.

	D_s^+ reconstruction D_s^+ decay mode					K^-	K_S^0	
Source	$\overline{\phi\pi^+}$	$K_S^0K^+$	$\bar{K}^*(892)^0K^+$	$ ho^+ \phi$	$\eta\pi^+(\gamma\gamma/\pi^+\pi^-\pi^0)$	$\eta'\pi^+(\gamma\gamma/\pi^+\pi^-\pi^0)$	<i>K</i> ⁻	K_S^0
K ID	2.20	1.10	2.20	2.20			1.10	
π ID	0.90		0.90	0.90	0.90/2.70	2.70/4.50		
Tracking	1.05	1.05	1.05	1.05	0.35/1.05	1.05/1.75	0.35	
$K_{\rm S}^0$ reconstruction		2.23						2.2
π^0 reconstruction				2.25	2.25/· · ·	2.25/· · ·		
Photon reconstruction					4.0/· · ·	4.0/⋅ ⋅ ⋅		
Mass windows of intermediate states	0.07	0.20	0.97	1.44	0.23/1.68	0.26/1.69		0.2
Bs of intermediate-state decays	0.08	0.08	0.08	1.12	0.04/0.03	0.04/0.03		
D_s^+ mass window	0.43	0.67	0.19	0.79	1.07	1.20		
D_s^{*+} mass window	0.38	1.01	0.10	0.34	0.94	0.61		

	Reconstruction mode					
Source	$D_s^+K^-$	$D_s^+ K_S^0$	$D_s^{*+}K^-$	$D_s^{*+}K_S^0$		
$D_s^{(*)+}K$ reconstruction	3.2	3.2	3.3	3.4		
$\mathcal{B}(D_s^{*+} o \gamma D_s^+)$		• • •	0.7	0.7		
Trigger	1.0	1.0	1.0	1.0		
MC statistics	0.2	0.2	0.2	0.2		
$N_{\Upsilon(2S)}$ (luminosity)	2.2(1.4)	2.2(1.4)	2.2(1.4)	2.2(1.4)		
Sum in quadrature	4.0(3.6)	4.0(3.6)	4.2(3.8)	4.2(3.9)		

TABLE III. The parameters $A = \sqrt{\sigma^{\rm B}(e^+e^- \to D_s^{(*)+}D_{sJ}^-)/\mathcal{B}(\Upsilon(2S) \to D_s^{(*)+}D_{sJ}^-)}$ from the results of the simultaneous fits and the maximum effect of interference term $F_{\rm int}^{\rm max}$ in the $\Upsilon(2S)$ decays. The values of $A(K^-)$ and $F_{\rm int}^{\rm max}(K^-)$ are for the K^- mode, and the values of $A(K_S^0)$ and $F_{\rm int}^{\rm max}(K_S^0)$ are for the K_S^0 mode.

	$D_s^+ D_{s1}(2536)^-$	$D_s^{*+}D_{s1}(2536)^-$	$D_s^+ D_{s2}^* (2573)^-$	$D_s^{*+}D_{s2}^*(2573)^-$
$A(K^{-})(nb^{1/2})$	2.05 ± 0.23	2.45 ± 0.38	2.00 ± 0.32	3.43 ± 0.99
$A(K_S^0)(nb^{1/2})$	2.00 ± 0.25	2.23 ± 0.38	1.98 ± 0.36	3.07 ± 0.94
$F_{\mathrm{int}}^{\mathrm{max}}(K^{-})(\%)$	8.0	9.7	8.0	14.4
$F_{\mathrm{int}}^{\mathrm{max}}(K_S^0)(\%)$	7.9	9.0	8.2	13.2

for both. We determine these total uncertainties of $\sum \varepsilon_i \times$ \mathcal{B}_i to be 3.2%, 3.2%, 3.3%, and 3.4% in the final states of $D_s^+ K^- \bar{D}^{(*)0}$, $D_s^+ K_S^0 D^{(*)-}$, $D_s^{*+} K^- \bar{D}^{(*)0}$, and $D_s^{*+} K_S^0 D^{(*)-}$, respectively. To estimate the systematic uncertainty in the angular distribution of $D_s^{(*)+}D_{s,I}^-$, we generate new MC samples uniformly in phase space, and half of the efficiency differences are taken to be the systematic uncertainties. We obtain the systematic uncertainties of 6.9%, 8.5%, 8.5%, and 9.2% for the $D_s^+D_{s1}(2536)^-$, $D_s^+D_{s2}^*(2573)^-$, $D_s^{*+}D_{s1}(2536)^-$, and $D_s^{*+}D_{s2}^{*}(2573)^-$, respectively. The uncertainty of the total number of $\Upsilon(2S)$ events is 2.2%. The uncertainties in the integrated luminosities for the two data samples are 1.4% and highly correlated, but they cancel in the scale factor. We estimate the systematic uncertainty in determining the $\mathcal{B}^{UL}(\Upsilon(2S) \rightarrow$ $D_s^{*+}D_{s2}^*(2573)^-)\mathcal{B}(D_{s2}^*(2573)^- \to K^-\bar{D}^0)$ to be $\delta_{sys} =$ 10.1%. Besides those listed in Table II, there are additional systematic uncertainties of the scale factor f_{scale} and the radiative correction factor $1+\delta_{\rm ISR}$, where ISR is the initial state radiation. By changing $s_{\text{cont}}/s_{\Upsilon(2S)}$ to $[s_{\text{cont}}/s_{\Upsilon(2S)}]^{1.5}$, the value of f_{scale} changes from 0.304 to 0.319, and we take 4.9% to be its systematic uncertainty. By varying the photon energy cutoff 50 MeV in the simulation of ISR, we determine the change of $1 + \delta_{ISR}$ to be 0.01 and take

1.0% to be the conservative systematic uncertainty. Various systematic uncertainties are considered in the simultaneous fit. We change the fit range from [2.51, 2.57] to [2.51, 2.62] GeV/ c^2 for the $D_{s1}(2536)^-$ signals, and from [2.50, 2.74] to [2.50, 2.79] GeV/ c^2 for the

 $D_{s2}^*(2573)^-$ signals. We vary the mass and width of $D_{s1}(2536)^-$ or $D_{s2}^*(2573)^-$ by 1σ according to the world average values [7]. We also change the mass resolutions from the signal MC simulations by 1σ , and the systematic uncertainties are found to be negligible.

We neglect the interference between the resonance and continuum amplitudes in $\Upsilon(2S)$ decays in the simultaneous fit since it cannot be determined from the available data samples with an unknown relative phase between the two amplitudes. Instead, we estimate the maximum effect $F_{\rm int}^{\rm max} \equiv \sigma_{\rm int}/(\sigma_{\rm int}+\sigma_{\Upsilon(2S)})$ according to the factor $A=\sqrt{\sigma^{\rm B}(e^+e^-\to D_s^{(*)+}D_{sJ}^-)/\mathcal{B}(\Upsilon(2S)\to D_s^{(*)+}D_{sJ}^-)}$ [17], and take it as the systematic uncertainty. Here $\sigma_{\Upsilon(2S)}$ and $\sigma_{\rm int}$ are the cross sections of the resonance process and the interference term in the $\Upsilon(2S)$ decays, respectively. We obtain the values $A\pm\Delta A$ from the fit results for $\sigma^{\rm B}(e^+e^-\to D_s^{(*)+}D_{sJ}^-)$ and $\mathcal{B}(\Upsilon(2S)\to D_s^{(*)+}D_{sJ}^-)$, which are listed in Table I, and then obtain $F_{\rm int}^{\rm max}$ with the input of

V. SUMMARY

 $A + \Delta A$, as shown in Table III.

In summary, we observe the charmed strange meson pair $D_s^{(*)+}D_{sJ}^-$ production in $\Upsilon(2S)$ decays and in e^+e^- annihilation at $\sqrt{s}=10.52$ GeV for the first time, where D_{sJ}^- is $D_{s1}(2536)^-$ or $D_{s2}^*(2573)^-$. We determine the products of branching fractions for the D_{sJ}^- production in $\Upsilon(2S)$ decays to be

$$\mathcal{B}(\Upsilon(2S) \to D_s^+ D_{s1}(2536)^-) \mathcal{B}(D_{s1}(2536)^- \to K^- D^*(2007)^0) = (1.6 \pm 0.3 \pm 0.2) \times 10^{-5},$$

$$\mathcal{B}(\Upsilon(2S) \to D_s^{*+} D_{s1}(2536)^-) \mathcal{B}(D_{s1}(2536)^- \to K^- D^*(2007)^0) = (1.4 \pm 0.4 \pm 0.2) \times 10^{-5},$$

$$\mathcal{B}(\Upsilon(2S) \to D_s^+ D_{s2}^*(2573)^-) \mathcal{B}(D_{s2}^*(2573)^- \to K^- D^0) = (1.4 \pm 0.4 \pm 0.2) \times 10^{-5},$$

$$\mathcal{B}(\Upsilon(2S) \to D_s^{*+} D_{s2}^*(2573)^-) \mathcal{B}(D_{s2}^*(2573)^- \to K^- D^0) = (0.9 \pm 0.5 \pm 0.2) \times 10^{-5},$$

and

$$\mathcal{B}(\Upsilon(2S) \to D_s^+ D_{s1}(2536)^-) \mathcal{B}(D_{s1}(2536)^- \to K_S^0 D^*(2010)^-) = (0.84 \pm 0.18 \pm 0.15) \times 10^{-5},$$

$$\mathcal{B}(\Upsilon(2S) \to D_s^{*+} D_{s1}(2536)^-) \mathcal{B}(D_{s1}(2536)^- \to K_S^0 D^*(2010)^-) = (0.82 \pm 0.25 \pm 0.19) \times 10^{-5},$$

$$\mathcal{B}(\Upsilon(2S) \to D_s^+ D_{s2}^*(2573)^-) \mathcal{B}(D_{s2}^*(2573)^- \to K_S^0 D^-) = (0.69 \pm 0.20 \pm 0.22) \times 10^{-5},$$

$$\mathcal{B}(\Upsilon(2S) \to D_s^{*+} D_{s2}^*(2573)^-) \mathcal{B}(D_{s2}^*(2573)^- \to K_S^0 D^-) = (0.54 \pm 0.31 \pm 0.47) \times 10^{-5}.$$

We also determine the upper limit $\mathcal{B}^{\text{UL}}(\Upsilon(2S) \to D_s^{*+}D_{s2}^*(2573)^-)\mathcal{B}(D_{s2}^*(2573)^- \to K^-\bar{D}^0) < 2.9 \times 10^{-5}$ and $\mathcal{B}^{\text{UL}}(\Upsilon(2S) \to D_s^{*+}D_{s2}^*(2573)^-)\mathcal{B}(D_{s2}^*(2573)^- \to K_S^0D^-) < 3.0 \times 10^{-5}$ at 90% C.L. We determine Born cross sections for continuum productions of the D_{s1}^- at $\sqrt{s} = 10.52$ GeV to be

$$\sigma^{\text{Born}}(e^{+}e^{-} \to D_{s}^{+}D_{s1}(2536)^{-})\mathcal{B}(D_{s1}(2536)^{-} \to K^{-}D^{*}(2007)^{0}) = (67 \pm 8 \pm 6) \text{ fb},$$

$$\sigma^{\text{Born}}(e^{+}e^{-} \to D_{s}^{*+}D_{s1}(2536)^{-})\mathcal{B}(D_{s1}(2536)^{-} \to K^{-}D^{*}(2007)^{0}) = (84 \pm 11 \pm 11) \text{ fb},$$

$$\sigma^{\text{Born}}(e^{+}e^{-} \to D_{s}^{+}D_{s2}^{*}(2573)^{-})\mathcal{B}(D_{s2}^{*}(2573)^{-} \to K^{-}D^{0}) = (56 \pm 9 \pm 13) \text{ fb},$$

$$\sigma^{\text{Born}}(e^{+}e^{-} \to D_{s}^{*+}D_{s2}^{*}(2573)^{-})\mathcal{B}(D_{s2}^{*}(2573)^{-} \to K^{-}D^{0}) = (106 \pm 17 \pm 12) \text{ fb},$$

and

$$\sigma^{\text{Born}}(e^{+}e^{-} \to D_{s}^{+}D_{s1}(2536)^{-})\mathcal{B}(D_{s1}(2536)^{-} \to K_{S}^{0}D^{*}(2010)^{-}) = (34 \pm 5 \pm 4) \text{ fb},$$

$$\sigma^{\text{Born}}(e^{+}e^{-} \to D_{s}^{*+}D_{s1}(2536)^{-})\mathcal{B}(D_{s1}(2536)^{-} \to K_{S}^{0}D^{*}(2010)^{-}) = (41 \pm 6 \pm 6) \text{ fb},$$

$$\sigma^{\text{Born}}(e^{+}e^{-} \to D_{s}^{+}D_{s2}^{*}(2573)^{-})\mathcal{B}(D_{s2}^{*}(2573)^{-} \to K_{S}^{0}D^{-}) = (27 \pm 6 \pm 5) \text{ fb},$$

$$\sigma^{\text{Born}}(e^{+}e^{-} \to D_{s}^{*+}D_{s2}^{*}(2573)^{-})\mathcal{B}(D_{s2}^{*}(2573)^{-} \to K_{S}^{0}D^{-}) = (51 \pm 11 \pm 9) \text{ fb}.$$

For comparison, $\sigma^{\rm Born}(e^+e^-\to \mu^+\mu^-)=0.784$ nb at $\sqrt{s}=10.52$ GeV and $\mathcal{B}(\Upsilon(2S)\to \mu^+\mu^-)=(1.93\pm0.17)\%$ [7]. We define the ratios $R_1\equiv\mathcal{B}(\Upsilon(2S)\to D_s^{(*)+}D_{sJ}^-)/\mathcal{B}(\Upsilon(2S)\to \mu^+\mu^-)$ for the $\Upsilon(2S)$ decays and $R_2\equiv\sigma^{\rm Born}(e^+e^-\to D_s^{(*)+}D_{sJ}^-)/\sigma^{\rm Born}(e^+e^-\to \mu^+\mu^-)$ for the continuum productions. We obtain $R_1/R_2=9.7\pm2.3\pm1.1$, $6.8\pm2.1\pm0.8$, $10.2\pm3.3\pm2.5$, and $3.4\pm2.1\pm0.8$ for

the $D_s^+ D_{s1}(2536)^-$, $D_s^{*+} D_{s1}(2536)^-$, $D_s^+ D_{s2}^*(2573)^-$, and $D_s^{*+} D_{s2}^*(2573)^-$ final states in the $D_{sJ}^- \to K^- \bar{D}^{(*)0}$ modes, respectively, where the uncertainty of $\mathcal{B}(\Upsilon(2S) \to \mu^+ \mu^-)$ is taken into account of the systematic uncertainties. The measured R_1/R_2 values indicate that the strong decay dominates in $\Upsilon(2S) \to D_s^{(*)+} D_{sJ}^-$ processes.

Here, we also determine the ratios of branching fractions to be

$$\mathcal{B}(D_{s1}(2536)^- \to K_s^0 D^*(2010)^-)/\mathcal{B}(D_{s1}(2536)^- \to K^- D^*(2007)^0) = 0.48 \pm 0.07 \pm 0.02,$$

 $\mathcal{B}(D_{s2}^*(2573)^- \to K_s^0 D^-)/\mathcal{B}(D_{s2}^*(2573)^- \to K^- D^0) = 0.49 \pm 0.10 \pm 0.02,$

which are in good agreement with the expected values of 0.498 and 0.497 from isospin symmetry, considering the phase space, since with K_S^0 only half of the neutral kaons can be reconstructed. The first ratio has the same precision as the world average value [7], while the second ratio is the first measurement of this quantity.

ACKNOWLEDGMENTS

This work, based on data collected using the Belle detector, which was operated until June 2010, was supported by the Ministry of Education, Culture, Sports, Science, and Technology (MEXT) of Japan, the Japan Society for the Promotion of Science (JSPS), and the Tau-Lepton Physics Research Center of Nagoya University; the Australian Research Council including Grants No. DP210101900, No. DP210102831, No. DE220100462, No. LE210100098, No. LE230100085; Austrian Federal Ministry of Education, Science and Research (FWF) and FWF Austrian Science Fund No. P 31361-N36; National Key R&D Program of China

under Contract No. 2022YFA1601903, National Natural Science Foundation of China and research Grants 11575017, No. 11761141009, No. 11705209, 11975076, No. 12135005, No. 12150004, No. 12161141008, and No. 12175041, and Shandong Provincial Natural Science Foundation **Project** No. ZR2022JQ02; the Ministry of Education, Youth and Sports of the Czech Republic under Contract No. LTT17020; the Czech Science Foundation Grant No. 22-18469S; Horizon 2020 ERC Advanced Grant No. 884719 and ERC Starting Grant No. 947006 "InterLeptons" (European Union); the Carl Zeiss Foundation, the Deutsche Forschungsgemeinschaft, the Excellence Cluster Universe, and the VolkswagenStiftung; the Department of Atomic Energy (Project Identification No. RTI 4002) and the Department of Science and Technology of India; the Istituto Nazionale di Fisica Nucleare of Italy; National Research Foundation (NRF) Grant Nos. 2016R1D1A1B02012900, No. 2018R1A2B3003643, No. 2018R1A6A1A06024970, RS202200197659, No. 2019R1I1A3A01058933,

No. 2021R1A6A1A03043957, No. 2021R1F1A1060423, No. 2021R1F1A1064008, No. 2022R1A2C1003993; Radiation Science Research Institute, Foreign Large-size Research Facility Application Supporting project, the Global Science Experimental Data Hub Center of the Korea Institute of Science and Technology Information, and KREONET/GLORIAD; the Polish Ministry of Science and Higher Education and the National Science Center; the Ministry of Science and Higher Education of the Russian Federation, Agreement 14.W03.31.0026, and the HSE University Basic Research Program, Moscow; University of Tabuk research Grants No. S-1440-0321, No. S-0256-1438, and No. S-0280-1439 (Saudi Arabia); the Slovenian Research Agency Grants No. J1-9124 and No. P1-0135; Ikerbasque, Basque Foundation for Science, Spain; the

Swiss National Science Foundation; the Ministry of Education and the Ministry of Science and Technology of Taiwan; and the U.S. Department of Energy and the National Science Foundation. These acknowledgements are not to be interpreted as an endorsement of any statement made by any of our institutes, funding agencies, governments, or their representatives. We thank the KEKB group for the excellent operation of the accelerator; the KEK cryogenics group for the efficient operation of the solenoid; the KEK computer group and the Pacific Northwest National Laboratory (PNNL) Environmental Molecular Sciences Laboratory (EMSL) computing group for strong computing support; and the National Institute of Informatics, and Science Information NETwork 6 (SINET6) for valuable network support.

^[1] N. Brambilla, S. Eidelman, C. Hanhart, A. Nefediev, C.-P. Shen, C. E. Thomas, A. Vairo, and C.-Z. Yuan, Phys. Rep. **873**, 1 (2020).

^[2] N. Brambilla et al., Eur. Phys. J. C 71, 1534 (2011).

^[3] H. Fritzsch and K. H. Streng, Phys. Lett. B **77**, 299 (1978).

^[4] B. Aubert *et al.* (*BABAR* Collaboration), Phys. Rev. D **81**, 011102 (2010).

^[5] D. Kang, T. Kim, J. Lee, and C. Yu, Phys. Rev. D 76, 114018 (2007).

^[6] Y. J. Zhang and K. T. Chao, Phys. Rev. D 78, 094017 (2008).

^[7] R. L. Workman *et al.* (Particle Data Group), Prog. Theor. Exp. Phys. **2022**, 083C01 (2022).

^[8] I. I. Y. Bigi and S. Nussinov, Phys. Lett. 82B, 281 (1979).

^[9] S. Kurokawa and E. Kikutani, Nucl. Instrum. Methods Phys. Res., Sect. A 499, 1 (2003), and other papers included in this volume; T. Abe *et al.*, Prog. Theor. Exp. Phys. 2013, 03A001 (2013) and references therein.

^[10] A. Abashian *et al.* (Belle Collaboration), Nucl. Instrum. Methods Phys. Res., Sect. A 479, 117 (2002); also see detector section in J. Brodzicka *et al.*, Prog. Theor. Exp. Phys. 2012, 04D001 (2012).

^[11] D. J. Lange, Nucl. Instrum. Methods Phys. Res., Sect. A 462, 152 (2001).

^[12] M. Ablikim et al. (BESIII Collaboration), Phys. Lett. B 846, 138245 (2023).

^[13] R. Brun *et al.*, GEANT3.21, CERN Report No. DD/EE/84-1,

^[14] E. Nakano, Nucl. Instrum. Methods Phys. Res., Sect. A 494, 402 (2002).

^[15] H. Nakano, Ph.D. thesis, Tohoku University, 2014.

^[16] M. Feindt and U. Kerzel, Nucl. Instrum. Methods Phys. Res., Sect. A 599, 190 (2006).

^[17] Y. P. Guo and C. Z. Yuan, Phys. Rev. D 105, 114001 (2022).

^[18] S. Actis et al., Eur. Phys. J. C 66, 585 (2010).

^[19] X. K. Dong, X. H. Mo, P. Wang, and C. Z. Yuan, Chin. Phys. C 44, 083001 (2020).

^[20] E. A. Kuraev and V. S. Fadin, Yad. Fiz. 41, 733 (1985) [Sov. J. Nucl. Phys. 41, 466 (1985)].

^[21] S. Jadach, B. F. L. Ward, and Z. Was, Phys. Rev. D 63, 113009 (2001); Comput. Phys. Commun. 130, 260 (2000).

^[22] M. Benayoun, S. I. Eidelman, V. N. Ivanchenko, and Z. K. Silagadze, Mod. Phys. Lett. A 14, 2605 (1999).